WARWICK
THE UNIVERSITY OF WARWICK

Original citation:
Petcher, P. A. and Dixon, S. (2016) Mode mixing in shear horizontal ultrasonic guided waves. Nondestructive Testing and Evaluation. ISSN 1058-9759 (In Press)

Permanent WRAP URL:
http://wrap.warwick.ac.uk/80794

Copyright and reuse:
The Warwick Research Archive Portal (WRAP) makes this work of researchers of the University of Warwick available open access under the following conditions.

This article is made available under the Creative Commons Attribution 4.0 International license (CC BY 4.0) and may be reused according to the conditions of the license. For more details see: http://creativecommons.org/licenses/by/4.0/

A note on versions:
The version presented in WRAP is the published version, or, version of record, and may be cited as it appears here.

For more information, please contact the WRAP Team at: wrap@warwick.ac.uk

warwick.ac.uk/lib-publications

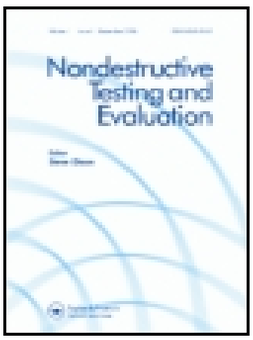

Nondestructive Testing and Evaluation

ISSN: 1058-9759 (Print) 1477-2671 (Online) Journal homepage: http://www.tandfonline.com/loi/gnte20

Mode mixing in shear horizontal ultrasonic guided waves

P. A. Petcher & S. Dixon

To cite this article: P. A. Petcher & S. Dixon (2016): Mode mixing in shear horizontal ultrasonic guided waves, Nondestructive Testing and Evaluation, DOI: 10.1080/10589759.2016.1184268

To link to this article: http://dx.doi.org/10.1080/10589759.2016.1184268

© 2016 The Author(s). Published by Informa UK Limited, trading as Taylor & Francis Group

Published online: 22 Jul 2016.

Submit your article to this journal

Article views: 38

View related articles

View Crossmark data

Full Terms & Conditions of access and use can be found at
http://www.tandfonline.com/action/journalInformation?journalCode=gnte20

Download by: [137.205.202.122] **Date:** 05 August 2016, At: 07:50

NONDESTRUCTIVE TESTING AND EVALUATION, 2016
http://dx.doi.org/10.1080/10589759.2016.1184268

Taylor & Francis
Taylor & Francis Group

Mode mixing in shear horizontal ultrasonic guided waves

P. A. Petcher and S. Dixon

Department of Physics, University of Warwick, Coventry, UK

ABSTRACT

SH guided waves are used increasingly for non-destructive testing (NDT) applications, particularly for pipes and pipe supports using circumferentially guided wave modes. In practical implementations, it is not always straightforward to ensure single-mode operation and this requires consideration when interpreting results. During shear horizontal (SH) wave generation or SH guided wave interaction with geometrical changes or defects, multiple SH guided wave modes may be produced, depending on the shear wave speed, the frequency of operation, the thickness of the sample and the transducer characteristics. This paper discusses the interference patterns created as the multiple SH modes mix (for both continuous tone generation and short bursts), and the problems caused by the interference patterns on applications such as NDT. In particular, the patterns can lead to defects being missed during an NDT inspection using SH waves, and a way to circumvent this problem is suggested.

ARTICLE HISTORY
Received 22 December 2015
Accepted 25 April 2016

KEYWORDS
Shear horizontal (SH) waves; guided waves; PPM EMAT; ultrasonics; NDT

Downloaded by [137.205.202.122] at 07:50 05 August 2016

1. Introduction

Shear waves oscillate perpendicular to their direction of propagation, and shear bulk waves can be classified into shear vertical (SV) waves, with a polarisation perpendicular to the surface plane and shear horizontal (SH) waves, with a polarisation parallel to the surface plane (the oscillation is in the in-plane direction).[1,2] The difference in polarisation is not as trivial as it first seems since it leads to differences in generation and detection of the waves, and in their propagation behaviour,[3] as well as how they interact with defects and interfaces (SH bulk waves do not undergo any mode-conversion when reflecting from a surface plane parallel to their polarisation, for example).[1,2] SH guided waves are, however, able to mode convert to other SH guided wave modes under certain geometrical conditions for particular ranges of frequencies. Some care is necessary when using SH waves, as although it is often the case that only a single wave mode is desired, the transducer may generate multiple SH guided wave modes in the sample, depending on the shear wave speed, the frequency of operation, the thickness of the sample or the presence of geometrical changes or defects in the sample and the transducer characteristics.

SH electromagnetic acoustic transducers (EMATs) are increasingly used for inspection of plates and pipe-like structures, including applications such as detecting corrosion,[4]

CONTACT S. Dixon s.m.dixon@warwick.ac.uk

© 2016 The Author(s). Published by Informa UK Limited, trading as Taylor & Francis Group.
This is an Open Access article distributed under the terms of the Creative Commons Attribution License (http://creativecommons.org/licenses/by/4.0/), which permits unrestricted use, distribution, and reproduction in any medium, provided the original work is properly cited.

Downloaded by [137.205.202.122] at 07:50 05 August 2016

weld inspection,[5] and thickness gauging.[6] It is well known that complications in data interpretation can arise if multiple modes are present in any guided wave inspection, and at the first stage, strategies to minimise this should be employed. An approach sometimes considered for limiting the number of different SH modes that can be generated involves driving the generation current of an SH EMAT at a frequency below the cut-off frequency of unwanted modes; and narrowing the bandwidth can also reduce production of multiple modes. For example, aiming to generate only the SH0 mode would require driving the SH EMAT at a frequency below that at which the SH1 mode would be generated. However, in practice, it is often not possible to use this approach to perform a meaningful SH EMAT inspection. There are various reasons for this, but the foremost one is that some inspection or measurement methods need to be able to generate and detect modes higher than the SH0 mode using the same probe on the same sample. Practical situations rarely offer the luxury of having a very wide range of EMATs with different wavelengths suited to every thickness of sample. In addition, field deployable and battery-powered equipment is often only capable of driving a current of a few cycles of a particular frequency, and the resultant bandwidth can easily excite multiple modes with the same wavelength, using the same EMAT.[6] In laboratory-based environments, it is often possible to employ methods to improve mode quality to a degree, but in many realistic inspection challenges it is not, and therefore it is important to firstly recognise the issue and then understand the problem. This paper is aimed at highlighting this problem.

Other steps to reduce the problems caused by multiple mode interaction would typically include increasing the separation between generation and detection point, or trying to ensure that the speeds of modes generated are significantly different. A problem not always considered is that the separation should have occurred at the point of interaction with the area (potentially containing a defect) under investigation; wave modes other than the lowest-order SH mode, SH0, are dispersive and have displacement fields that vary with depth (SH0 is uniform throughout the thickness of the sample),[1,2] leading to interference patterns that vary through the sample thickness. Due to these interference patterns, it is possible, for example, that a defect could be missed or incorrectly interpreted during a non-destructive testing (NDT) inspection using SH waves. Also, an inspection is often seeking to measure features such as wall loss by corrosion, where the thickness of the sample can vary by an unknown amount. This changes the dispersion curves significantly, in an unpredictable way when the level of corrosion is unknown. Under certain conditions, SH guided waves can mode convert to different SH guided wave modes when there is a change in sample thickness, or another discontinuity such as a crack. Again, this can give rise to multiple SH modes being generated at arbitrary positions, with no control possible from the user.

There is a misconception amongst some researchers that SH guided wave modes do not mode convert when interacting with defects.[7] This probably stems from earlier work correctly stating that SH bulk waves do not mode convert when incident on a boundary. Subsequent research has shown clearly that SH guided waves can and do mode convert in realistic inspection geometries.[8]

This paper presents a strategy for modelling and identifying some of the type of wave modes that can arise as a result of SH guided wave mode mixing. The simulation work is then validated using experimental measurements, showing some of the effects that can be observed when undertaking SH guided wave inspection of plates or plate-like structures.

2. SH guided wave dispersion curves

There are multiple symmetric and anti-symmetric SH guided wave modes; the phase and group speeds are dependent on the frequency, sample thickness, and the bulk shear wave speed.[1,2] For a frequency, f, a plate of thickness d, and a bulk shear wave speed, c_s, the phase (c_p), and group (c_g) speeds are given by [2]:

$$c_p = 2c_s(fd)/\sqrt{4(fd)^2 - n^2c_s^2} \tag{1}$$

$$c_g = c_s\sqrt{1-(n/2)^2/[(fd)/c_s]^2} \tag{2}$$

The cut-off frequency-thickness for each mode is given by:

$$(fd)_n = nc_s/2 \tag{3}$$

For symmetric modes, n is an even integer (0, 2, 4, …), and for anti-symmetric modes, n is an odd integer (1, 3, 5, …). Note that for $n = 0$, $c_p = c_g = c_s$ for all frequencies, making it non-dispersive. As $(fd) \to \infty$, the speed of any mode approaches c_s. Example dispersion curves are given in Figure 1.

The displacements for the symmetric (u_s) and anti-symmetric (u_a) SH modes, of angular frequency $\omega = 2\pi f$, propagating along a direction x and into a thickness d a distance $-d/2 \le y \le d/2$ (with $y = 0$ being at the centre of the sample thickness), are (A_n is a scaling value for each mode) [2]:

$$u_s = A_n \cos(\pi n y/d)\cos(\omega[t - x/c_p]) \tag{4}$$

$$u_a = A_n \sin(\pi n y/d)\cos(\omega[t - x/c_p]) \tag{5}$$

The displacement fields across the thickness of the plate do not vary along any mode's dispersion curve.[2] Example displacement curves are given in Figure 2. With regard to sensitivity to defect detection, and considering only a single wave mode, were a defect located near a position where the maximum displacement is zero (such as the centre of the sample

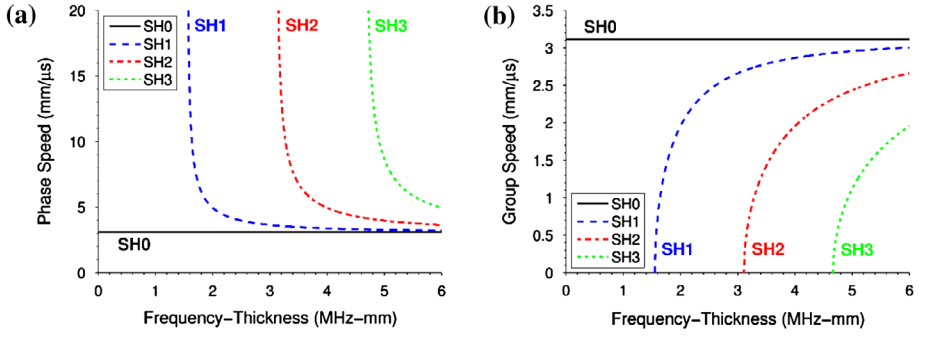

Figure 1. Analytical phase (a) and group (b) speed dispersion curves for SH guided waves in a flat plate. The shear wave speed is 3111 m/s (standard for aluminium [9]), and four modes are visible. SH0 is non-dispersive, with a speed equal to the shear wave speed.

Downloaded by [137.205.202.122] at 07:50 05 August 2016

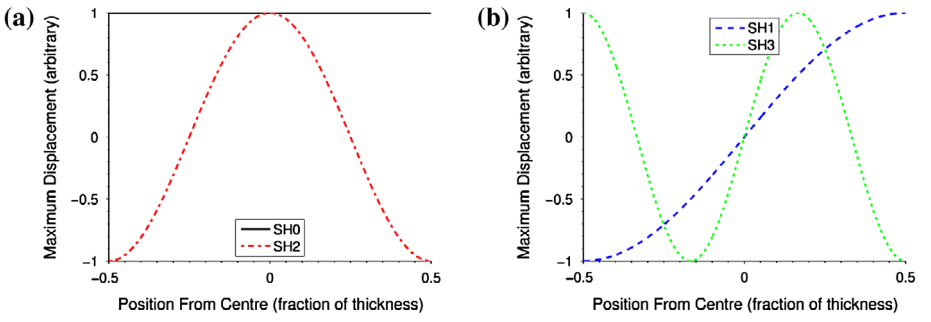

Figure 2. Displacement curves for symmetrical (a) and anti-symmetrical (b) modes. These curves do not include the time (t) and position (x) dependent terms, only the depth (y) dependent term. With the exception of the $n = 0$ mode, all of the modes will have the opposite displacement at some points and zero displacement at others. Therefore, a given mode may not be effective at detecting defects at certain depths.

Downloaded by [137.205.202.122] at 07:50 05 August 2016

thickness for SH1 and other antisymmetric modes), that defect would lead to a scattered SH wave with less energy than if it were located in a region with a larger maximum displacement.

3. Periodic-permanent-magnet EMATs

SH waves are not as simple to generate as SV or compression waves, but using a periodically varying array of permanent magnets, and a racetrack coil (a coil running in the direction of the periodicity), a periodic-permanent-magnet electromagnetic acoustic transducer (PPM EMAT) can be produced that can both generate and detect SH waves in a conducting sample.[10–12] An example of such a magnet array is shown in Figure 3. This paper does not concern itself with the operating principles of PPM EMATs, which are well covered in the existing literature,[10,13–15] except to state that the magnet array leads to a corresponding periodic variation in the in-plane shear forces generated at and just below the sample surface, when a current is pulsed through the coil. PPM EMATs are used for the experiments conducted for this paper, and the SH generation source was modelled within the simulations as a series of forces with a spatial periodic variation.

The magnet array periodicity has a wavelength, but the array has a finite length (and therefore a spatial bandwidth [6]), and the wavelength is only 'fixed' parallel to the surface plane whilst the EMAT generates SH energy in all directions within the sample. Therefore, the wavelength leads to the PPM EMAT having a dominant wavelength for generation and detection, but modes can be generated and detected away from these values. If a fixed wavelength, λ, and thickness, d, are assumed (this allows the replacement $f = c_p/\lambda$), the frequency, group and phase speed, of a given wave mode, is:

$$f(n) = c_s \sqrt{1/\lambda^2 + n^2/4d^2} \tag{6}$$

$$c_p = c_s \sqrt{1 + n^2\lambda^2/4d^2} \tag{7}$$

$$c_g = c_s \sqrt{1 - 1/(1 + 4d^2/n^2\lambda^2)} \tag{8}$$

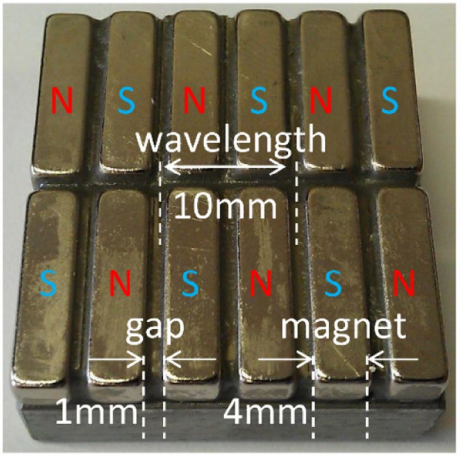

Figure 3. A PPM EMAT under construction; shown is the periodic array of magnets. The magnet polarisation varies periodically, as indicated by the N and S referring to the magnetic north and south poles. A racetrack coil is placed over this array, and a current pulsed through the coil will induce eddy currents in the sample. The eddy current will interact with the static magnetic field, creating a Lorentz force, which then generates SH waves.

The frequencies obtained by Equation (6) are used in simulations as the generation frequency, and experimentally as the initial (and often final) frequency tried when attempting to optimise the generation amplitude of an SH wave using PPM EMATs.

4. Simulating SH guided waves

Simulations were carried out using both a simple method based upon the dispersion curves described by Equation (1), and using the software PZFlex, which is an explicit time-domain finite element method (FEM) solver for ultrasonic wave propagation. PZFlex uses rectangular or cuboid mesh elements of uniform size for 2D or 3D models, respectively. This sometimes means that a higher density of elements is required to guarantee a sufficient number of elements per wavelength to ensure convergence of the model, when compared to other FE software models that can use triangular or tetrahedral meshing of variable size. However, calculation times for simple rectangular elements can be faster, and models are very simple to create with such a mesh. Built-in FE code for the absorbing boundary layers was used at the ends of the sample, and the performance of this code has been verified to perform satisfactorily. PZFlex is also used extensively in academic research to model multifarious ultrasonic phenomena, and if readers require any further detailed technical information they should consult the readily available technical documentation from the software developers (Weidlinger Associates Inc.).

4.1. Semi-analytic model creation

The semi-analytic model is simply the superposition of the displacements for the SH modes:

$$S = \sum_{n=0}^{N} u_n \tag{9}$$

Downloaded by [137.205.202.122] at 07:50 05 August 2016

Where u_n is the appropriate symmetric (u_s) or anti-symmetric (u_a) displacement from Equations (4) and (5) for each mode n. From those equations, $A_s = 1$ and $A_a = 1$ (initially), and c_p is set by Equation (1) using $c_s = 3111$ m/s, $f = 311.1$ kHz, and the same depth, d, as used in Equations (4) and (5). For each simulation, $-d/2 \leq y \leq d/2$, 0 mm $\leq x \leq$ 100 mm and 0 μs $\leq t \leq$ 100 μs. A thickness range of 1 mm $\leq d \leq$ 40 mm is considered. This equation provides output in two spatial dimensions, and time. The next stage is to window the output along the time dimension (a Hann window was chosen for this purpose), and perform a conversion to the analytic signal using a Hilbert transform.[16] The magnitude of the centre time point is then taken (the absolute value of the analytic signal at that temporal point), and the other time data discarded. It is the case that the window function will alter the magnitude found, but as long as the window is applied consistently (to the same length signal), and the magnitude taken from the same point (the centre time value), then magnitude values for different values of x, y and d can be compared against each other; the units for the magnitude are arbitrary in any case, as the values of A_s and A_a are set empirically by comparison to the output of the FEM model.

The purpose of this model is to provide a rough estimate of the relative magnitudes of the different wave modes present in an observed interference pattern generated by the FEM model described in the next section. This is achieved by modifying the values of A_s and A_a until an acceptable match with the FEM simulation is obtained. No effort is made in this work to provide a physical basis for the values of A_s and A_a, as this model is only intended as providing complementary information alongside the FEM model.

4.2. FEM model creation

The PZFlex simulation was two dimensional in terms of propagation, with the SH oscillation occurring in the third dimension (the software is capable of fully three-dimensional simulations, but that was not required in this case). The sample was modelled as an isotropic homogeneous aluminium plate, with no damping (approximating it as a linear elastic material), a density of 2698 kg/m^3, a bulk compression wave speed of 6374 m/s, a shear wave speed of 3111 m/s and a node every 0.01 mm (the FEM grid was discretised into square elements with sides of length 0.01 mm). The sample length was 200 mm, with a line of antisymmetry at one side (the zero point for that dimension); the antisymmetry gave an effective length of 400 mm. All other sides had free boundaries. The thickness was allowed to vary in the range 1 mm $\leq d \leq$ 40 mm. In the third dimension (in which the SH oscillation occurs), the plate is considered infinite. The PPM EMAT was modelled so that its centre point was along the line of antisymmetry; this meant that only half of the EMAT was explicitly modelled, with the simulation software assuming the other half was antisymmetric. A 10 mm wavelength was used for the EMAT model, as this is a common size used experimentally. Forces were applied in the positive z-direction (where z is the third dimension in which the SH wave oscillates) to the nodes at X positions of 0.5 to 4.5 mm, and 10.5 to 14.5 mm and forces in the negative z-direction were applied to the nodes at X positions of 5.5 to 9.5 mm. Due to the line of antisymmetry, this is mirrored on the other side of the line (see Figure 4). This is not a perfect representation of a PPM EMAT, but it is a sufficient approximation of the in-plane SH forces [6] to produce a useful model. The forces applied were of the form $\sin(2\pi ft)$, and the SH0 generation frequency was always 311.1 kHz (obtainable from Equation (6) which reduces to $f = c_s/\lambda$ for SH0), as this has no dependence on thickness. The application of the

Downloaded by [137.205.202.122] at 07:50 05 August 2016

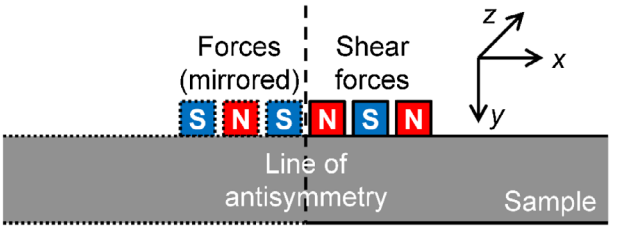

Figure 4. The FEM model uses a line of antisymmetry to reduce the area that requires simulation.

force leads to the generation of SH waves in the modelled sample at the excitation point, and these waves then propagate into the sample. The displacement in the *z*-direction with time was recorded for all nodes within the sample region, for a time period of 100 μs, at a sampling frequency of 500 MHz.

Having obtained the simulation results, as with the semi-analytic model, a conversion to the analytic signal using a Hilbert transform [16] is performed, but unlike for the semi-analytic case, a window is not applied. The signal has a natural start as the wave energy spreads into the sample, and is therefore already effectively windowed at the start time, and the simulation time is sufficiently long for problems not to occur at the times of interest due to the end of the signal not being windowed. The analytic signal is converted to a signal magnitude (the absolute value of the analytic signal). After transformation, a region of time is selected over which the magnitude can be seen to be steady (50 to 100 μs is generally safe), and the median magnitude taken over that time region (the median is to remove any fluctuations due to the magnitude not having fully stabilised). It was checked that the simulation had converged by repeating certain test cases at a 10th of the spatial resolution; these test cases were found to produce the same outputs to sufficient accuracy (visually they appear identical to those performed at the standard spatial resolution, and they are numerically very similar with a median difference of less than 1%).

5. Mixing of SH guided wave modes

There are many applications where it is desirable to generate only a single SH mode, but a simple examination of Equation (1) shows that as the frequency-thickness increases, there is an ever increasing number of modes that could be generated. Although a PPM EMAT may be optimised for a particular wavelength, that does not prevent other wavelengths of SH waves from being generated (particularly with a short tone burst), at amplitudes that are easily large enough to interfere significantly with the SH mode of interest.

5.1. Continuous tone input

The result of multiple SH modes being generated and propagating along the sample is that an interference pattern is generated. The pattern will first be considered for a PPM EMAT with a continuous tone input. This will make the pattern clear and easy to compare against the semi-analytic model. Once the existence and basis for such a pattern is established, the extent to which this applies to a shorter pulse can be investigated. The plots shown in Figure 5 are generated by FEM simulations, and represent the maximum wave displacement

Downloaded by [137.205.202.122] at 07:50 05 August 2016

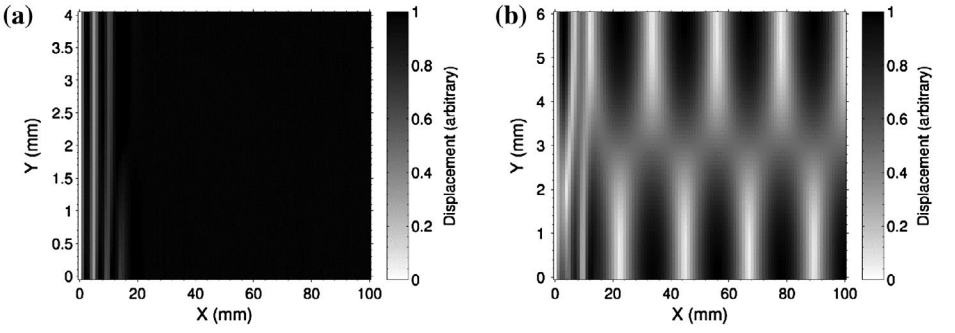

Figure 5. FEM simulations for samples of thickness 4 mm (a) and 6 mm (b). The input frequency was 311.1 kHz. At 4 mm, only the SH0 mode is present, but at 6 mm, the SH1 mode has clearly appeared as well. The cut-off frequency for the SH1 mode at 5 mm (the thickness in-between the two plots) is 311.1 kHz, and the SH1 mode does start to appear at that thickness.

Downloaded by [137.205.202.122] at 07:50 05 August 2016

magnitude that has been recorded at that point in the sample (in the z-direction) once the SH waves have propagated through the sample and the system has steadied. Close to the generation point and approximately for $X < 20$ mm, the guided wave has not yet been properly established and can be thought of as the near field in this case. Note that in the figures in this and the following sections, the node displacement magnitudes (the absolute value of the analytic signal obtained via Hilbert transform) in the SH oscillation direction are shown, not instantaneous node displacements (amplitudes). Another way of thinking of this is perhaps that the colour-coded amplitude displayed in each point of the image is a record of the maximum displacement amplitude recorded in the sample at that point, as the guided wave has propagated along the sample in the increasing X direction. Each figure's colour scale has been adjusted to range from zero to one, via the simple method of dividing the data by the maximum recorded value in the region 20 mm $\leq X \leq$ 100 mm, $0 \leq Y \leq d$, where X is the lateral distance from the centre of the PPM EMAT, and Y is the depth into the sample. The first 20 mm of the X dimension is ignored for scaling purposes, as this section is directly below the modelled PPM EMAT, leading to near-field effects. A discussion of these near-field effects is beyond the scope of this paper, and they exist in a region which would not typically be the subject of an inspection; generally the inspection region would be in front (20 mm $\leq X \leq$ 100 mm) or behind (-20 mm $\geq X \geq -100$ mm) the PPM EMAT, rather than directly below it (-20 mm $\leq X \leq$ 20 mm). Note that 20 mm has been chosen based upon empirical observations of the data sets shown in this paper; beyond this distance, the near-field effects appear to have no significant impact upon the pattern observed. More generally, the near-field distance can vary considerably depending on the parameters of the transducers, the pulse and the sample.

Considering the 4-mm thick sample in Figure 5(a), the majority of the plot is black and uniform, which demonstrates that the ultrasonic displacement magnitudes of the simulation nodes, due to the SH0 mode, are uniform through both the thickness and length dimension of the plate. The uniformity through the thickness indicates that no other wave modes are present, as expected since the frequency-thickness is below the cut-off for any other modes. When a 6-mm thick sample is modelled, both the SH0 and SH1 modes are observed, as can be seen in Figure 5(b). When both modes are present, a series of fringes are seen, with the

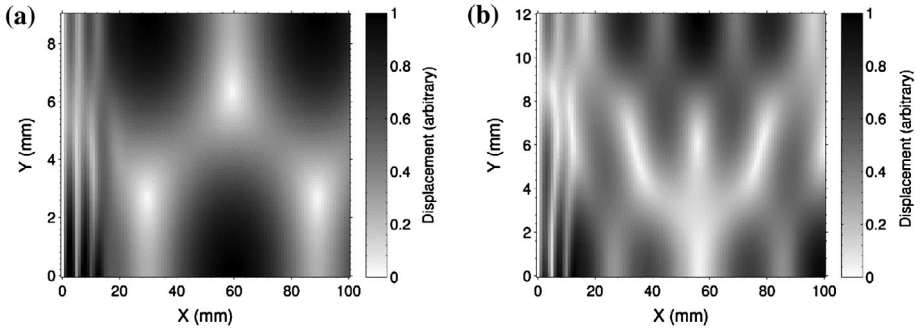

Figure 6. FEM simulations for samples of thickness 9 mm (a) and 12 mm (b). The input frequency was 311.1 kHz. At 9 mm, the SH0 and SH1 modes are present, but at 12 mm, the SH2 mode has appeared as well. The cut-off frequency for the SH2 mode at 10 mm is 311.1 kHz, and the SH2 mode does start to appear at that thickness.

Downloaded by [137.205.202.122] at 07:50 05 August 2016

low-magnitude regions having around 5% of the magnitude of the high-magnitude regions; like the SH1 mode, these fringes are antisymmetric about the centre ($Y = 3$) of the sample.

As with the SH1 mode, if the generation frequency is 311.1 kHz, the associated thickness at which the SH2 first exists is 10 mm. A FEM simulation of a 9-mm thick sample, Figure 6(a), again shows the antisymmetric fringes marking the presence of SH0 and SH1, as the frequency-thickness is below the cut-off for the SH2 mode. When a 12-mm thick sample is modelled, the SH0, SH1 and SH2 modes are present, as can be seen in Figure 6(b). With all three modes present (SH0 and SH2 are symmetric, SH1 is antisymmetric), the resulting pattern is more complicated. Relative to the highest magnitude region at zero depth, the low-magnitude region at the maximum depth has around 3% of the magnitude.

The output of the semi-analytic models was very close to the FEM for every modelled thickness described in Figures 5 and 6, and this is shown in Figure 7 for the 6 mm (a) and 12 mm (b) cases. Since the semi-analytic model only outputs the chosen wave modes, this strongly suggests that Figures 5(b) and 6(a) do only contain SH0 and SH1 modes (in roughly equal parts, as $A_0 = 1$ and $A_1 = 1$ provided a good match), and Figure 6(b) does contain SH0, SH1, and SH2 modes ($A_0 = 1$, $A_1 = -2$, and $A_2 = 1$ provided a good match, suggesting the SH1 mode has twice the magnitude of the SH0 and SH2 modes). As previously mentioned, this model provides no physical basis for the scaling values they are simply chosen to provide a good match with the FEM model in order to gain an estimate of the relative magnitudes of the different SH modes.

5.2. Tone burst (pulse) input

Usually SH waves are generated by a tone burst rather than by a continuous tone, as in many applications the time of flight of a wave is useful to ascertain, and this is far easier with a temporally short pulse. For the tone burst input, a pulse of four cycles has been used (at the same 311.1 kHz frequency as for the continuous case). As with the continuous tone case, it is necessary to obtain the signal magnitude at each point in the sample. The same conversion to the analytic signal using a Hilbert transform [16] is performed, and again, a window is not necessary. Since the generation input is a tone-burst, the signal has a natural

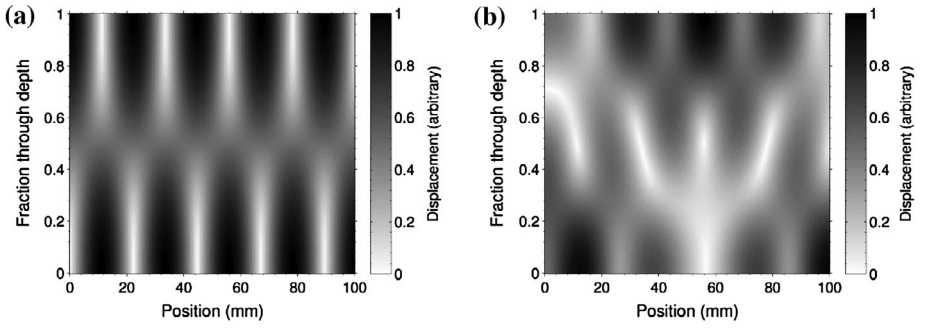

Figure 7. Semi-analytic models for samples of thickness 6 mm (a) and 12 mm (b). The input frequency was 311.1 kHz for all modes. At 6 mm, the SH0 and SH1 modes have been modelled, with an SH1 phase speed of 5628 m/s and scaling values of $A_0 = 1$ and $A_1 = 1$. At 12 mm, the SH0, SH1, and SH2 modes have been modelled, with a SH1 phase speed of 3422 m/s and a SH2 phase speed of 5628 m/s, and scaling values of $A_0 = 1$, $A_1 = -2$, and $A_2 = 1$. With these values for frequency, and the scaling values stated (which were set empirically), the similarity to the FEM simulations in Figures 5(b) and 6(b) is very close.

Downloaded by [137.205.202.122] at 07:50 05 August 2016

start and end, and is therefore already effectively windowed at both the start and end time. The analytic signal is converted to a signal magnitude as before. However, taking a median value of the magnitude is no longer possible, as any magnitude observed is transient, existing only when the wave passes. Instead, the maximum magnitude over the entire time period simulated is extracted. A brief discussion of this choice is warranted. For the continuous tone input, taking the median magnitude (where the magnitude of a complex signal is not the same as the instantaneous amplitude) will produce almost the same value as the maximum magnitude (again, not instantaneous amplitude); the variation is only due to error in the model and initial transients as the generation starts (as such an ideal case should be steady, so ideally median magnitude should equal maximum magnitude). The transient case can't use the median, because it changes with time, but using the maximum magnitude of the time-varying complex signal shows the greatest magnitude that any given region experiences, and that is often the quantity of interest in an inspection scenario.

As with the continuous tone figures, node displacement magnitudes (the absolute value of the analytic signal) are shown, not instantaneous node displacements (amplitudes). Each figure's colour scale has been adjusted to range from zero to one, via the simple method of dividing the data by the maximum value in the region 20 mm $\leq X \leq$ 100 mm, $0 \leq Y \leq d$. The first 20 mm of the X dimension is ignored for scaling purposes, as this section contains the modelled PPM EMAT, leading to near-field effects.

The pulsed counterparts to the continuous tone Figures 5 and 6 are Figures 8 and 9 (all FEM simulations); in general, although the patterns are weaker for the pulsed case, they are still present. Considering first Figure 5(a), there appears to be a pattern characteristic of some SH1 component being present. This is most likely due to the short input pulse having a large bandwidth (a continuous tone having a very narrow bandwidth). The result of the larger bandwidth is that some energy is at a high enough frequency to produce SH1 waves in addition to the SH0 waves. Figure 8(b) has the same pattern as Figure 5(b), although in the pulsed case, the fringes are slightly further apart. In addition, at the far right of Figure 8(a) and (b), the magnitude decreases. Figure 9(a) and (b) are good matches for Figure 6(a) and (b), respectively, but in the pulsed case, the patterns are weaker and more distorted than for

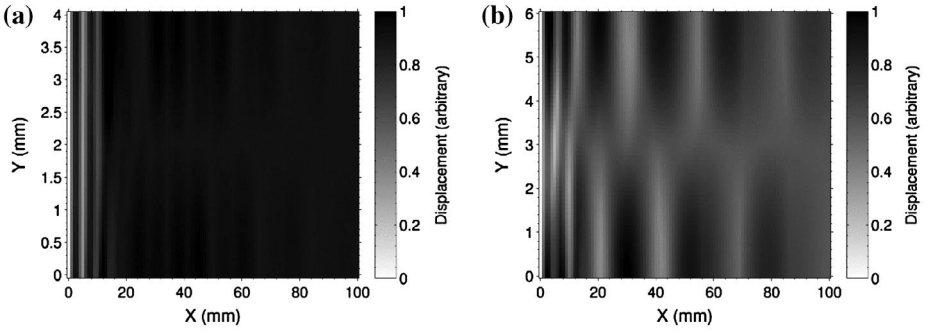

Figure 8. FEM simulations for samples of thickness 4 mm (a) and 6 mm (b). The input was a 4-cycle tone burst at a frequency of 311.1 kHz.

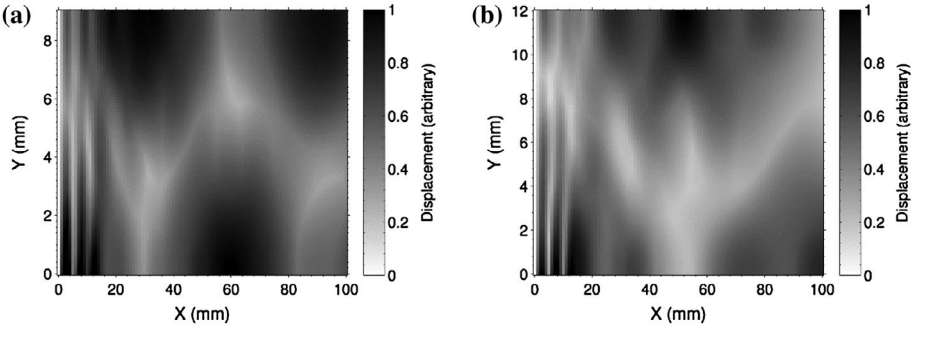

Figure 9. FEM simulations for samples of thickness 9 mm (a) and 12 mm (b). The input was a 4-cycle tone burst at a frequency of 311.1 kHz.

Downloaded by [137.205.202.122] at 07:50 05 August 2016

the continuous case. Considering Figures 6(b) and 9(b), relative to the highest magnitude region at zero depth, the low-magnitude region at the maximum depth has around 3% of the magnitude for the continuous case, and around 25% of the magnitude for the pulsed case.

Example A-scans are shown in Figures 10 and 11. These A-scans are taken from the FEM simulation of a 9-mm thick sample, and are the waves detected at positions of 30, 60 and 90 mm along the surface ($Y = 0$ mm) from the generation PPM EMAT centre point. A summary of the peak-to-peak amplitudes measured at detection points along the $Y = 0$ mm surface, the $Y = 9$ mm surface and between the two surfaces (the centre of the sample, $Y = 4.5$ mm), is also shown. It can be seen that at troughs in the peak-to-peak amplitude ($X = 30$ mm and $X = 90$ mm, corresponding to Figures 10(a) and 11(a)), the wave slightly dips in amplitude at its middle (at 15 and 30 μs, respectively); this dip is not evident at peaks in the peak-to-peak amplitude ($X = 60$ mm), corresponding to Figure 10(b).

Figures 10(a) and 11(a) appear similar, and looking at just one of these figures, it might be thought that this indicates that the modes are temporally separating. However, Figures 10(b) and 11(b) demonstrate that this 'separation' occurs cyclically, and it just due to an interaction between the modes. At this thickness, the group speeds of the two modes is similar (3111 m/s for SH0 and 2720 m/s for SH1), and a clear separation would not occur until approximately 0.5 m from the generation EMAT (a greater distance than is available for many inspections). There is another issue caused by the bandwidth of the pulse.

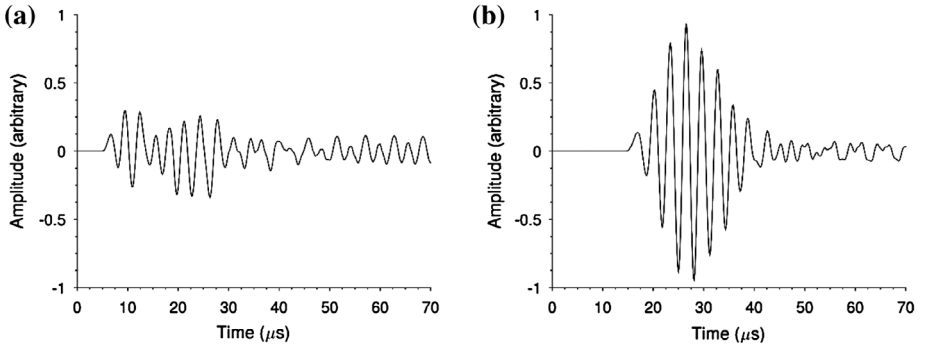

Figure 10. FEM simulations for a sample of thickness 9 mm. The input was a 4-cycle tone burst at a frequency of 311.1 kHz. This is the amplitude measured at positions 30 mm (a) and 60 mm (b) along the surface from the centre of the simulated PPM EMAT.

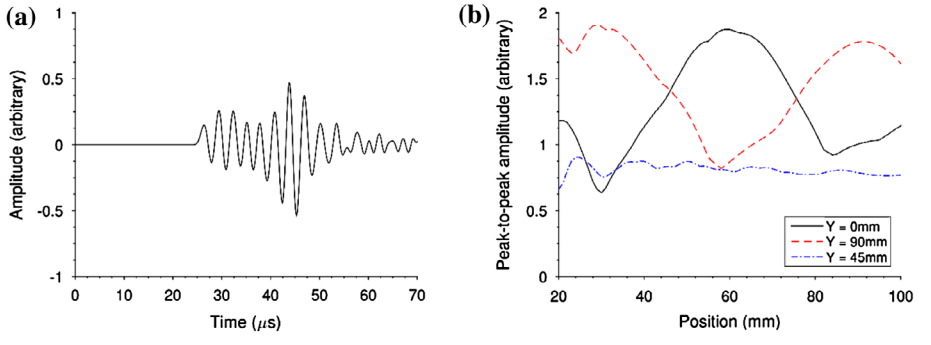

Figure 11. FEM simulations for a sample of thickness 9 mm. The input was a 4-cycle tone burst at a frequency of 311.1 kHz. The A-scan (a) is the amplitude measured at a position 90 mm along the surface from the centre of the simulated PPM EMAT. The summary of the peak-to-peak amplitudes (b) is for the zero depth surface.

Considering first a thin sample of 1 mm thickness, at the generation point where the PPM EMAT is placed, it is possible to use an EMAT/pulse with sufficient bandwidth to produce (for example) an SH0 and SH1 wave simultaneously, even if the centre frequency is 311.1 kHz. However, once they are propagating, the SH waves do not have sufficient bandwidth to generate any other wave modes. Therefore, if in a simulation the instantaneous displacements for a pure SH0 mode at 311.1 kHz were reproduced at an arbitrary point along the length of the sample, when the simulation were allowed to step forward in time, the SH0 mode would propagate, but no other modes would be seen; this is because the (spatial/temporal) bandwidth of the propagating modes would not be sufficient in this case to generate any other modes, as the frequency cut-off for an SH1 mode at that thickness is 1556 kHz. Consider now a 9-mm thick sample, using the same pulse as for the thin sample case. If the instantaneous displacements for a pure SH0 wave at 311.1 kHz were reproduced at an arbitrary point along the length of the sample (this being a uniform displacement through the thickness), when the simulation was allowed to step forward in time, an SH1 mode would appear, as the SH1 mode has a frequency cut-off of 173 kHz for that thickness of sample; the SH0 displacements are capable of generating an SH1 mode if they are at a

Downloaded by [137.205.202.122] at 07:50 05 August 2016

frequency above the cut-off. Therefore, the modes could only separate temporally if the SH0 mode generated has a frequency below the SH1 frequency-thickness cut-off, otherwise the SH0 propagation itself can generate the SH1 mode, a circumstance under which it is clear that the modes could not separate. As the sample becomes thicker, this problem becomes more severe; a 12 mm thick sample has a SH1 frequency cut-off of 130 kHz, and at 22 mm thick (a thickness that SH wave inspections are being investigated at [5]), the cut-off is only 71 kHz. At these frequencies, SH0 generation with a 10 mm wavelength PPM EMAT would be quite inefficient; 71 kHz would be an optimal frequency for a PPM EMAT with a 44 mm wavelength, and the same six PPM elements would be an unwieldy 132 mm long in total at that wavelength. Therefore, unless ever larger PPM EMATs were used as the thickness increases, the modes separating temporally cannot be relied upon, and the interference patterns shown within this paper must be accounted for.

These interference patterns must be considered in applications where a particular displacement field is required. For example, when SH waves are used to inspect a weld,[5] if there was a very low-magnitude displacement at the position of a defect, it could be missed by the inspection. A pulsed FEM simulation at 8-mm sample thickness was run (8 mm was chosen as samples of this thickness are more readily available than 9-mm thick samples), with the addition of a 3-mm or 1-mm vertical slot (extending along the *Y*-dimension from zero). The slot was placed at either 23 mm or 46 mm along the *X*-dimension, within the first low-magnitude and high-magnitude regions, respectively. The slot was 1-mm wide (in the *X*-dimension). As the addition of the slot means that the model is no longer antisymmetric about the zero point, the asymmetric boundary was removed and the FEM model extended such that all of Figure 4 was simulated directly. In addition, an extra step was introduced into the processing. First, the same simulation was run without a slot present, and the signal data were converted to a signal magnitude the same as for the other data. However, before the maximum magnitude over the entire time period is extracted, the signal magnitudes from the simulation without a slot are subtracted from the signal magnitudes generated from the simulations with a slot, so that the increase in signal magnitude in a region due to the effect of scattering by the slot can be seen.

Comparing Figure 12(a) and (b), it can be seen that if a slot is present in a region that has a low-magnitude region (23 mm along the *X*-dimension on the zero depth side of the sample), that the wave scattered from that region is also low in magnitude compared to if a slot is present in a region that has a relatively high magnitude (46 mm along the *X*-dimension on the zero depth side of the sample). This strongly suggests that for thicker plates, the position of the slot in both the *X* and *Y* dimensions is important, due to the interference pattern created by multiple wave modes being generated. It can also be seen from Figure 12 that the interference pattern scattered back is similar to the original interference pattern.

The standard interference pattern for an 8-mm thick sample (without a slot present), and a summary of the peak magnitude at the surface for slots of different depths, is provided in Figure 13. From, this, it can be seen that the scattered signal from the slot is in general much higher when the slot is in a high-magnitude region of the original interference pattern, compared to when the slot is in a low-magnitude region. In addition, the magnitude at the surface fluctuates as the interference pattern from the multiple SH modes is still present. There is a potential way of circumventing this problem. If the interference pattern for a given sample is known (the shear wave speed and the wave frequency are generally known, but the sample thickness may not be to sufficient precision, especially if considering

Downloaded by [137.205.202.122] at 07:50 05 August 2016

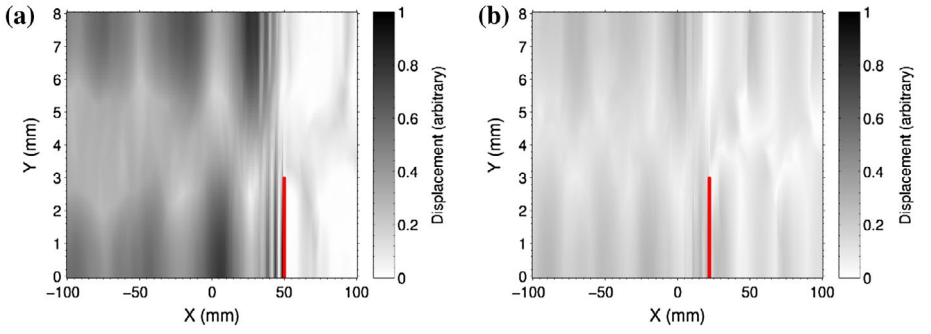

Figure 12. FEM simulations for samples of thickness 8 mm with 3 mm vertical (extending from 0 mm to 3 mm in the *Y*-dimension) slots at 46 mm (a) and 23 mm (b) in the *X*-dimension, and a 1 mm width in the *X*-dimension. The input was a 4-cycle tone burst at a frequency of 311.1 kHz. The incident wave magnitude has been removed by subtraction of a reference model without a slot present. The colour scale has been set so that 1 represents the peak magnitude present in (a), a peak that (b) does not reach. The slot position is marked by a red line.

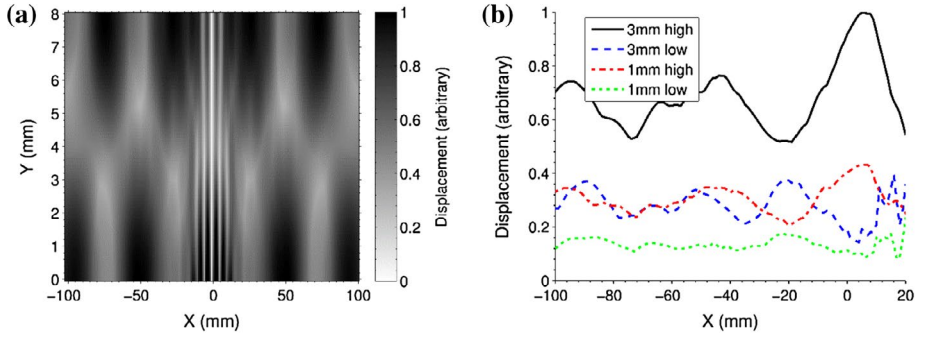

Figure 13. FEM simulation for a sample of thickness 8 mm without any slots (a). The input was a 4-cycle tone burst at a frequency of 311.1 kHz. A summary of results (b) is also provided. The summary is the peak magnitude at the surface the simulated EMAT is on, after the subtraction of the incident magnitude, for the 3 and 1 mm slot cases, when those slots are in 'high' or 'low' magnitude regions of the interference pattern. The slot is at $X = 46$ mm for the 'high' case and at $X = 23$ mm for the 'low' case. The X range for (b) is mostly negative, as the generation EMAT (with centre at zero X) is close to the slot, so the detection EMAT is assumed to be behind it (at negative X).

corrosion), it can be predicted where the low-magnitude regions will appear. The PPM EMAT generator can then be positioned such that the region of interest in the sample is covered by a high-magnitude region, and the EMAT can be moved again if a large region of interest is to be covered. Alternatively, if the interference pattern is not known, a range of generation positions can simply be tried, until the slot is in a high-magnitude region. The scattered signal can sometimes also be predicted, and the detection PPM EMAT positioned accordingly, but even if such a prediction cannot be made, the detection PPM EMAT can be scanned over a distance large enough to include at least one high-magnitude section.

There is a possible advantage to the existence of the interference pattern, if it is reasonably well known. A defect can generally be located laterally by scanning the PPM EMATs across the area of interest,[5] and in terms of distance (in the propagation direction) by the

Downloaded by [137.205.202.122] at 07:50 05 August 2016

wave time of flight, and by moving the generation EMAT, the defect can be brought into high- and then low-magnitude regions of the interference pattern. If, for example, it is known that at the distance the defect is being examined at, that the surface on which the EMAT sits has a high-magnitude region, and the opposite surface a low-magnitude region, then if the defect provides a small response at that distance, it can be inferred that the defect is closer to the opposite surface to the one the EMAT sits upon. However, this process would become difficult at larger frequency-thickness values, as the interference pattern is more complicated, and so it is not something that could be used in inspections generally.

6. Experimental verification

The existence of the patterns for short tone bursts has been tested experimentally. Two SH PPM EMATs were used, each consisting of six alternating elements (such as in Figure 3 and modelled in Figure 4) with a wavelength of 10 mm. A RITEC RPR-4000 pulser/receiver provided the generation pulses, and the filtering and amplification of the received signal. The generation pulse was at a frequency of 311.1 kHz (optimised for SH0 at a 10 mm wavelength), and consisted of a 4- or 8-cycle current burst. The received signal was band-pass filtered by the RITEC RPR-4000, with a high-pass cut-off of 0.2 MHz, and a low-pass cut-off of 2.5 MHz. The signals are digitised by a PC equipped with a GaGe Octopus 8482 Express CompuScope card sampling at 25 MHz. After digitisation, the signal is time-gated to the region of interest, a brick-wall band-pass frequency filter is applied (the pass-band is from 200 to 800 kHz, a band in which almost all the signal energy is present), and conversion to an analytic signal using a Hilbert transform [16] is performed. As with the pulsed FEM simulations, a window is not necessary, since the generation input is a tone-burst, and the signal has a natural start and end. As with the FEM simulation for a pulsed input, the maximum magnitude for the time period of interest (the region selected by time gating) is calculated.

The test sample was an aluminium plate of dimensions 400 mm × 300 mm with a (8 ± 0.05) mm thickness. A generation EMAT was placed on the surface. A detection EMAT was placed 50 mm away from the front face of the generating EMAT, in the direction of the SH wave propagation, and measurements were taken in 2 mm increments moving away from the generation EMAT, to a total separation of 200 mm. At each position, 64 averaged measurements are taken. The initial configuration is shown in Figure 14.

Following that experiment, an approximately 3-mm deep vertical slot is machined into the surface of the sample, and the generation and detection EMATs are moved so that they are on the same side of the slot (Figure 15). The distance to the slot and the distance between the EMATs are then varied to investigate the influence of the guided wave pattern on defect detection.

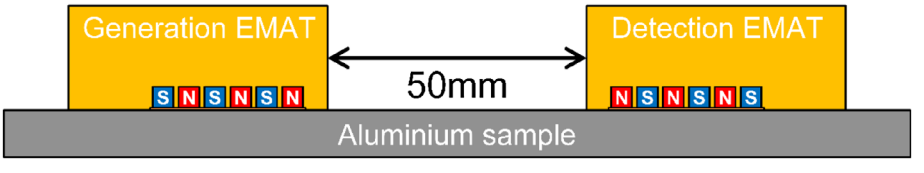

Figure 14. The basic configuration of the experiment to confirm the guided wave patterns generated. PPM EMATs with a 10 mm wavelength are used on an 8 mm thickness aluminium sample. The detection EMAT is moved away from its initial position in 2 mm increments to a final separation of 200 mm.

Downloaded by [137.205.202.122] at 07:50 05 August 2016

The results of these experiments demonstrate that the interference pattern exists, and that it leads to a change in the magnitude of waves scattered from a slot. It can be seen from Figure 16(a) (the experiment without a slot depicted in Figure 14) that the interference pattern is clearly more significant for the eight-cycle case, as would be expected; if both wave modes exist for a larger number of cycles, the start and end of the pulse is less relevant. Unlike the two-dimensional simulations, the experiment is fully three dimensional, and the geometric spreading out of the SH wave results in a downward trend in the detected magnitude. Figure 16(b) provides a comparison to a pulsed FEM simulation at 8 mm sample thickness, although the limited extent of the simulation (due to the time and PC memory constraints under which the simulation was carried out), means that the detection position extends only from 50 to 100 mm. Despite this limitation, the similarity between the simulation and the experiment is clear, with both the change in magnitude (relative to the peak magnitude) and the detection position over which it occurs matching up well. The simulation uses only a four-cycle tone burst, but it maintains the interference pattern as well as the eight-cycle tone burst experiment; this is possibly due to the simulation being in two

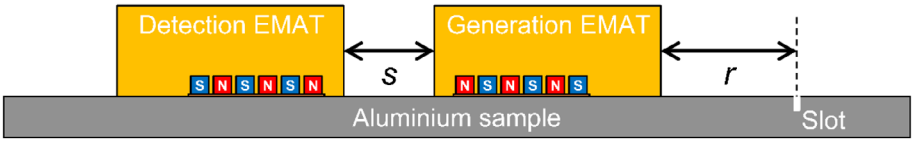

Figure 15. The basic configuration of the experiment to investigate the effect of the guided wave patterns on defect detection. PPM EMATs with a 10 mm wavelength are used on an 8 mm thickness aluminium sample, and the slot is approximately 3 mm deep. The distance *r* is varied so that the reflected energy from a slot in a high- and low-amplitude region of the displacement field can be observed, and the distance *s* is varied to confirm that the detection EMAT does not enter a low-amplitude displacement field region as *r* is varied.

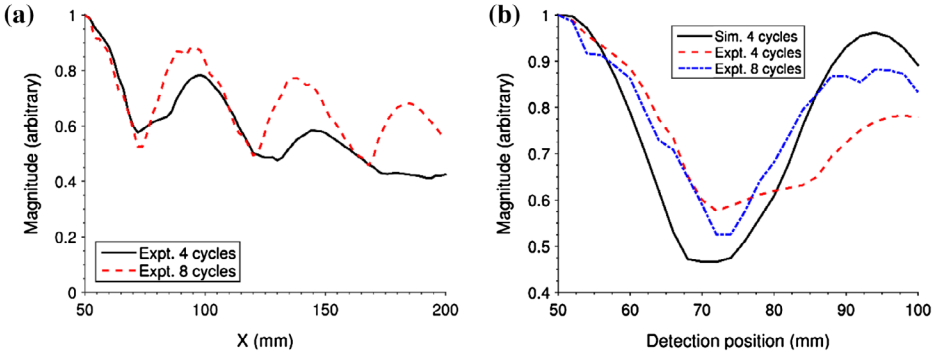

Figure 16. Results for the experiment depicted in Figure 14, with a sample of thickness 8 mm, and a comparison to the simulated data. The input was at a frequency of 311.1 kHz (optimised for SH0 at a 10 mm wavelength). A scan as the detection PPM EMAT is moved (using either a 4- or 8-cycle tone burst, indicated in the legend) shows a clear oscillation in the peak magnitude detected (a). A pulsed FEM simulation at 8 mm sample thickness was run as a comparison (b), although only over the detection positions from 50 to 100 mm due to time and PC memory constraints. There is a close similarity in both the change in magnitude and the detection range over which the change takes place (note that the legend indicates experimental and simulation data as 'Expt.' and 'Sim.', respectively).

Downloaded by [137.205.202.122] at 07:50 05 August 2016

dimensions rather than three, as well as the idealised nature of the simulated generation EMAT, and the point-like nature of the detection point (the experiment uses another PPM EMAT for detection). Other differences from the simulated scenario include the pulser used to generate the pulse experimentally, which in general will not output as ideal a tone burst as used in the simulation, and the sample, which may have slightly different properties from those simulated; these could also lead to the dissimilarities observed.

Example A-scans comparing the experimental and simulated data are shown in Figures 17 and 18. The simulated A-scans are taken from the FEM simulation of an 8-mm thick sample, and are the waves detected at positions of 50, 70 and 94 mm along the surface (zero depth) from the generation PPM EMAT centre point. Experimental A-scans at these same detection positions have waveforms that match reasonably. Again, it can be seen that at a trough in the peak-to-peak amplitude (a detection position of 70 mm, corresponding to Figure 17(b)), the wave slightly dips in amplitude at its middle (at approximately 33 μs); this dip is not evident at peaks in the peak-to-peak amplitude (detection positions of 50 and

Downloaded by [137.205.202.122] at 07:50 05 August 2016

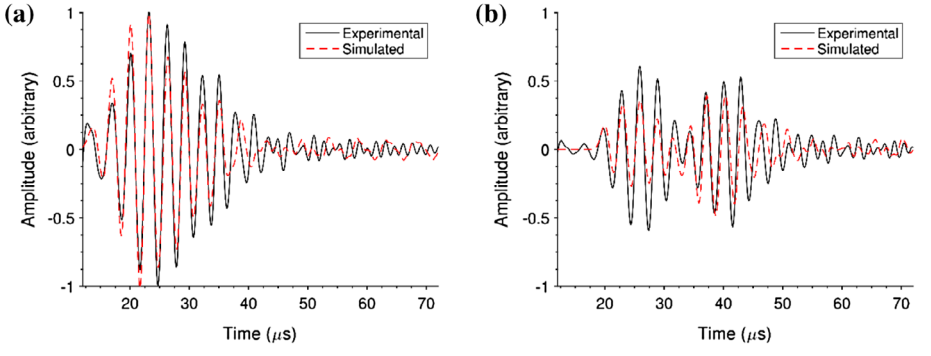

Figure 17. Comparison of experimental and simulation results for the experiment depicted in Figure 14, with a sample of thickness 8 mm. The input was a 4-cycle tone burst at a frequency of 311.1 kHz. The A-scans shown are for detection positions of 50 mm (a) and 70 mm (b).

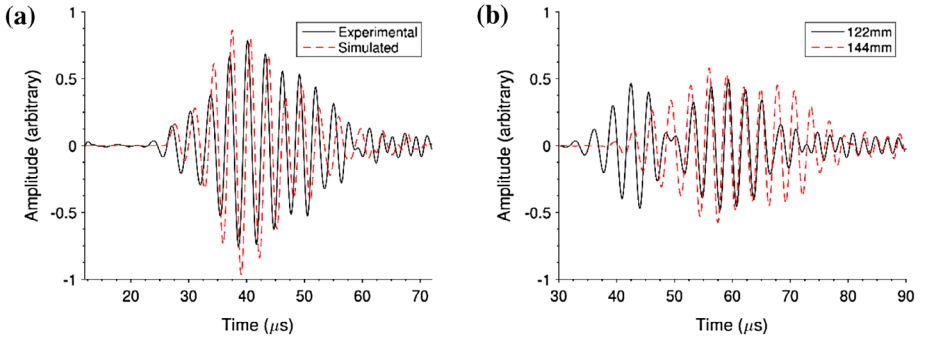

Figure 18. Comparison of experimental and simulation results for the experiment depicted in Figure 14, with a sample of thickness 8 mm, and a detection position of 94 mm (a). Also shown are experimental results at detection positions of 122 mm and 144 mm (b), demonstrating that the same pattern of a single continuous waveform (144 mm) and a waveform with a dip in the middle (122 mm) is repeated at larger detection distances. The input was a 4-cycle tone burst at a frequency of 311.1 kHz.

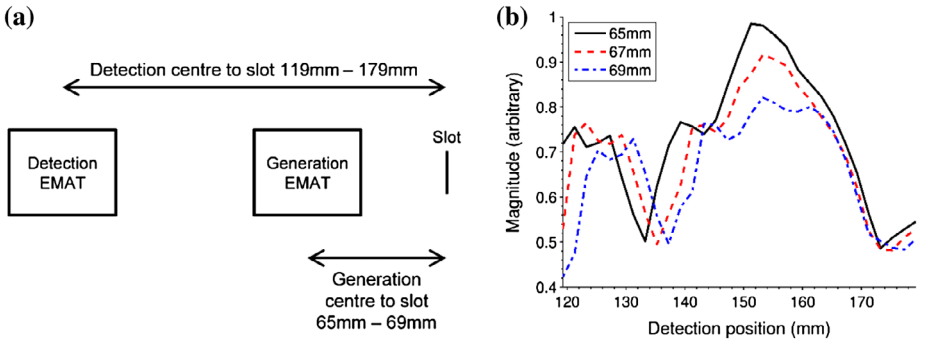

Figure 19. Results for the experiment depicted in Figure 15, with a sample of thickness 8 mm. The input was at a frequency of 311.1 kHz, using a 4-cycle tone burst. The diagram (a) shows the change in generation position (65 to 69 mm) and the change in detection position (119 to 179 mm) represented by the legend and horizontal scale, respectively, of (b). As the generation PPM EMAT is moved, the peak magnitude detected changes due to the slot being in a region of the interference pattern with a lower magnitude, as can be seen from the equivalent simulation (Figures 12 and 13).

Downloaded by [137.205.202.122] at 07:50 05 August 2016

94 mm, corresponding to Figures 17(a) and 18(a), respectively). Again, there is no clearly distinct SH1 mode present, and this is also the case in Figure 18(b), which contains only experimental data at positions of 122 and 144 mm, provided here to demonstrate that the pattern shown in Figure 17 continues at larger distances from the generation point.

Figure 19 (the experiment with a slot depicted in Figure 15) demonstrates that as the generation EMAT position (given by the legend) is moved, the peak magnitude decreases, but the interference pattern remains as the detection EMAT position (given by the horizontal axis) changes. The change in peak magnitude is not as dramatic as that in the simulated results of Figure 13, but it is still present, and could be more pronounced for a deeper slot, or for a slot with a narrower opening (the opening in this case was 0.5 mm due to the limitations of the machining equipment available). The same time and PC memory constraints that limited the comparison with simulated data shown in Figure 16(b), makes a comparison with this data difficult, beyond a basic comparison of the peak magnitude values since the detection positions used in the experiment are beyond the equivalent ranges for the 'low' case and only overlapping to a small extent for the 'high' case. Comparing the peak values in the simulated 100 to 80 mm detection position range (which is as far as the simulation extends in the negative direction, representing a position behind the generation point), to those in the experiment, the simulation shows a 50% drop in peak value, whereas the experiment shows an approximate 17% drop in peak value. It was observed in Figure 16 that for the four-cycle tone burst experiment, the interference pattern is less significant, but this was not observed for the simulation, most likely due to the idealised nature of the simulation. A four-cycle tone burst was used to collect the data in Figure 19, and the equivalent simulation also used a four-cycle tone burst; again the idealised nature of the simulation, including the extremely narrow width of the simulated slot, is the most likely cause for the greater significance of the interference pattern on the results. Unfortunately, the experiment could not in this case use an eight-cycle tone burst, as the size of the sample meant that reflections from waves scattering off the sample edges interfered with the waves scattered by the slot when the data capture time was extended to accommodate reception

of the longer pulse. Despite this, it can be clearly seen that it is not just the interference of the modes at the detection EMAT that is important, but also their interference at the point of interaction with the defect.

7. Conclusions

SH guided waves are often difficult to generate in a single mode due to restrictions on the availability of PPM EMAT wavelengths for different thicknesses of different materials, and by bandwidth limitations due to both the electronics that is used to drive the generation transducer, and the need for a short pulse such that any scattered pulses can be temporally separated from outgoing pulses (if generation to target separation is in any way limited). In addition to these issues, geometrical changes in the sample or defects such as cracks or corrosion patches of unknown size and location can give rise to mode conversion of the SH guided wave, and this can lead to the SH guided wave mode mixing. The mixing of SH guided wave modes leads to interference patterns within the bulk of a sample, which can occur whether the source is a continuous tone or a tone burst (a pulse).

Using a combination of finite element modelling, semi-analytical modelling and experimental validation, we have demonstrated some of the effects that can be observed in these SH guided wave inspection measurements, and some of the implications of failure to recognise the presence of mixed modes. This is particularly important as the use of SH guided waves in plant inspection is becoming increasingly commonplace. Finite element modelling allows for a view within the (sometimes complicated geometry) sample that cannot be achieved experimentally, and the semi-analytical modelling allows for an estimation (by comparison with the finite element model) of the relative amplitudes of each wave mode, thus demonstrating that the phenomena observed is due to the expected wave modes, and not any other wave modes.

The existence of these interference patterns means that in the first instance the interference of mixed modes must be recognised in applications using guided SH waves, such as NDT inspections. We have shown that changes in the expected temporal profiles of the received waves, or oscillations in the amplitude with a change in sensor position, are indicative of possible mode mixing. Failure to recognise the presence of these mixed modes would result in unexpected results, such as normally detectable defects being missed during the inspection. However, by being aware of the likely interference patterns, steps can be taken to circumvent the problems, ensuring that SH guided waves can remain a useful inspection tool over a wide frequency-thickness range.

Downloaded by [137.205.202.122] at 07:50 05 August 2016

Acknowledgements

The authors are very grateful to the project partners, Rolls-Royce and National Nuclear Laboratory (NNL), for providing additional funding, and to AMEC, for supplying the sample.

Disclosure statement

No potential conflict of interest was reported by the authors.

Funding

This work was supported by the Engineering and Physical Sciences Research Council (EPSRC), grant EP/I03160X/1, through the Research Centre in Non-destructive Evaluation (RCNDE).

ORCID

P. A. Petcher http://orcid.org/0000-0002-7526-5156

References

[1] Graff KF. Wave motion in elastic solids. New York: Dover Publications; 1975.
[2] Rose JL. Ultrasonic waves in solid media. Cambridge: Cambridge University Press; 1999.
[3] Petcher PA, Burrows SE, Dixon S. Shear horizontal (SH) ultrasound wave propagation around smooth corners. Ultrasonics. 2014;54:997–1004.
[4] Andruschak N, Saletes I, Filleter T, Sinclair A. An NDT guided wave technique for the identification of corrosion defects at support locations. NDT & E Int. 2015;75:72–79.
[5] Petcher PA, Dixon S. Weld defect detection using PPM EMAT generated shear horizontal ultrasound. NDT & E Int. 2015;74:58–65.
[6] Dixon S, Petcher Y, Fan Y, et al. Ultrasonic metal sheet thickness measurement without prior wave speed calibration. J. Phys. D: Appl. Phys. 2013;46:445502.
[7] Gauthier J, Mustafa V, Chahbaz A. EMAT generation of polarized shear waves for pipe inspection. In: Pan American Conference for Nondestructive Testing. Proceedings; 1998. Toronto (ON), Canada. Available from: www.ndt.net/article/pacndt98/40/40.htm.
[8] Nurmalia. Mode conversion behaviour of SH guided wave in a tapered plate. NDT & E Int. 2012;45:156–161.
[9] Kaye GWC. Tables of physical and chemical constants (web edition) - the speed and attenuation of sound; 2004. Available from: http://www.kayelaby.npl.co.uk/general_physics/2_4/2_4_1.html.
[10] Vasile CF, Thompson RB. Excitation of horizontally polarized shear elastic waves by electromagnetic transducers with periodic permanent magnets. J. Appl. Phys. 1979;50:2583–2588.
[11] Hirao M, Ogi H. An SH-wave EMAT technique for gas pipeline inspection. NDT & E Int. 1999;32:127–132.
[12] Ogi H, Goda E, Hirao M. Increase of efficiency of magnetostriction SH-wave electromagnetic acoustic transducer by angled bias field: piezomagnetic theory and measurement. Jpn. J. Appl. Phys. Part 1 – Regular Papers Short Notes & Review Papers. 2003;42:3020–3024.
[13] Silk MG. Ultrasonic transducers for nondestructive testing. Bristol: Adam Hilger; 1984.
[14] Hirao M, Ogi H. EMATs for science and industry: noncontacting ultrasonic measurements. London: Kluwer Academic; 2003.
[15] Ohtsuka Y, Higashi M, Nishikawa M. Fundamental experiment for inspection of cooling pipes in operation by using ultrasonic technique. Fusion Eng. Design. 2006;81:1583–1587.
[16] Marple SL. Computing the discrete-time "analytic" signal via FFT. IEEE Trans. Signal Process. 1999;47:2600–2603.

Downloaded by [137.205.202.122] at 07:50 05 August 2016